




Effective elastic moduli of composites with a strongly disordered host materialD. A. Conyuh , A. A. Semenov, and Y. M. Beltukov **Ioffe Institute, Politechnicheskaya Str. 26, 194021 St. Petersburg, Russia* (Received 30 March 2023; revised 2 August 2023; accepted 19 September 2023; published 20 October 2023)

The local elastic properties of strongly disordered material are investigated using the theory of correlated random matrices. A significant increase in stiffness is shown in the interfacial region, the thickness of which depends on the strength of disorder. It is shown that this effect plays a crucial role in nanocomposites, in which interfacial regions are formed around each nanoparticle. The studied interfacial effect can significantly increase the influence of nanoparticles on the macroscopic stiffness of nanocomposites. The obtained thickness of the interfacial region is determined by the heterogeneity lengthscale and is of the same order as the lengthscale of the boson peak.

DOI: [10.1103/PhysRevE.108.045004](https://doi.org/10.1103/PhysRevE.108.045004)**I. INTRODUCTION**

Amorphous glassy materials exhibit spatially inhomogeneous microscopic elastic properties due to their disordered structure [1–4]. The local elastic heterogeneity results in non-affine deformations of amorphous solids under uniform stress. The presence of nonaffine deformations was observed in a wide range of amorphous materials: metallic glasses [5], polymer hydrogels [6], supercooled liquids [7], Lennard-Jones glasses [8], and silica glass [9]. The typical lengthscale of nonaffine deformations was estimated as tens of particle sizes for Lennard-Jones glasses [10]. For smaller lengthscales, the classical continuum elasticity theory cannot be applied [11].

If the size of an amorphous medium is much larger than its heterogeneity lengthscale, one can use the macroscopic elastic moduli to describe the mechanical properties of this system. However, in composite systems containing amorphous materials, some regions may have small typical sizes. An important example is nanocomposites, in which the size of nano-inclusions may be comparable to the heterogeneity lengthscale of the host amorphous medium. Therefore, it is important to study the local elastic properties of amorphous solids, especially near the interface with other materials.

Amorphous polymers are an important class of amorphous materials. The elastic properties of polymer nanocomposites attract considerable interest due to their unique properties and great potential as future materials [12–15]. It was established that doping a polymer with nanoparticles, even at low concentrations, could lead to significant changes in the elasticity of the host material [16–20].

It was proposed that the elastic properties of nanocomposites can be described by the so-called three-phase model [21]. The model assumes that the structure of a polymer is perturbed around the nanoparticle, which results in an effective interphase region around the nanoparticle with intermediate elastic properties. The interphase region has a strong influ-

ence on the macroscopic stiffness of the nanocomposite due to the large total surface area of nanoparticles. At present, the three-phase model is usually used as a phenomenologic model to fit the influence of inclusions on macroscopic elastic moduli obtained experimentally or using molecular dynamics [22–27].

Recent molecular-dynamics studies have directly shown an increase in local elastic moduli of epoxy near the boehmite nanolayer [28] and polystyrene near the silica nano-inclusion [29]. In the latter case, an increase in polystyrene stiffness was revealed within a characteristic range of 1.4 nm from the nanoparticle, while polystyrene density saturates to the bulk value at significantly shorter distances. The enhancement of the local elastic properties of the polymer was attributed to the effect of nonaffine deformations, which requires a more detailed theoretical study.

It was shown that the general vibrational and mechanical properties of amorphous solids can be studied by the random matrix model [30,31]. Recently, using the theory of correlated random matrices, the analytical form of the vibrational density of states and the dynamical structure factor was obtained [32].

In the present paper, the theory of correlated random matrices is applied to study the effect of disorder on local elastic properties.

II. LINEAR RESPONSE

Macroscopic elastic properties determine the relationship between the macroscopic strain of a system and the applied macroscopic stress. In the general case, a linear response to some external force f_i acting to the i th degree of freedom of the system at frequency ω is determined by the following equation:

$$\sum_j [\Phi_{ij} - \omega^2 m_{ij}] u_j = f_i, \quad (1)$$

where u_j is the displacement of the j th degree of freedom from the equilibrium position, \hat{m} is the mass matrix (usually it is a diagonal matrix, but we are not limited to this case),

*ybeltukov@gmail.com

and $\hat{\Phi}$ is the force-constant matrix. The latter is defined by the second derivatives of the total interatomic interaction energy $U(x_1, x_2, \dots)$ at the equilibrium as

$$\Phi_{ij} = \frac{\partial^2 U}{\partial x_i \partial x_j}, \quad (2)$$

where x_i is the coordinate, which corresponds to the i th degree of freedom. In three-dimensional system with N_a atoms, there are $N = 3N_a$ degrees of freedom.

Particular equilibrium coordinates x_1, x_2, \dots, x_N depend on the cooling process of the glass forming system. Therefore, there are different realizations of the force-constant matrix $\hat{\Phi}$ for different equilibrium configurations. Thus, the force-constant matrix has a random nature.

Equation (1) shows how the force-constant matrix $\hat{\Phi}$ determines the linear response u_i due to external forces. Although the response u_i is different for each realization of $\hat{\Phi}$, the fluctuations of macroscopic quantities based on u_i (e.g., the macroscopic strain) are negligible. Therefore, it is important to find the average reaction $\langle u_i \rangle$, which can be expressed from Eq. (1) in the next form:

$$\langle u_i \rangle = - \sum_j G_{ij}(\omega^2) f_j, \quad (3)$$

where the resolvent

$$\hat{G}(z) = \left\langle \frac{1}{\hat{m}z - \hat{\Phi}} \right\rangle \quad (4)$$

is introduced. The angular brackets denote the averaging over different realizations of $\hat{\Phi}$, and z is a complex number. The relation between the average response $\langle u_j \rangle$ and the forces f_i can be expressed as

$$\sum_j [\Phi_{ij}^{\text{eff}}(\omega^2) - \omega^2 m_{ij}] \langle u_j \rangle = f_i, \quad (5)$$

where $\hat{\Phi}^{\text{eff}}$ is the effective force-constant matrix, which can be written using the resolvent $\hat{G}(z)$ as

$$\hat{\Phi}^{\text{eff}}(z) = \hat{m}z - \hat{G}(z)^{-1}. \quad (6)$$

The study of the effective force-constant matrix $\hat{\Phi}^{\text{eff}}$ is the main goal of the present paper. In such an analysis, the difference in each realization of $\hat{\Phi}$ must be taken into account. Note that for a strongly disordered system, the matrix $\hat{\Phi}^{\text{eff}}$ may significantly differ from the mean force-constant matrix $\langle \hat{\Phi} \rangle$. To find the properties of $\hat{\Phi}^{\text{eff}}$, we use the random matrix theory, which is based on the general properties of amorphous solids.

III. RANDOM MATRIX APPROACH

The presence of disorder in amorphous systems leads to the random nature of the force-constant matrix elements Φ_{ij} . Therefore, the random matrix theory can be applied to study the effects of disorder in such systems. However, we are interested in mechanically stable systems, which exhibit a small response due to small external forces. It means that the force-constant matrix $\hat{\Phi}$ has to be positive-semidefinite. Also, Φ_{ij} is symmetric, which follows from (2). As a result, there are complicated correlations between the matrix elements Φ_{ij} .

The above-mentioned conditions are equivalent to the possibility to represent $\hat{\Phi}$ in the form

$$\hat{\Phi} = \hat{A}\hat{A}^T, \quad (7)$$

where \hat{A} is some rectangular matrix [33]. It leads to the positive-definite quadratic potential energy of the system [34], which can be presented as $U = \sum_k U_k$, where

$$U_k = \frac{1}{2} \left(\sum_i A_{ik} u_i \right)^2. \quad (8)$$

Thus, the potential energy of the system may be described by a number of positive-definite bonds enumerated by the index k .

The matrix \hat{A} can be interpreted as follows. The i th row of the matrix \hat{A} corresponds to the i th degree of freedom, and the k th column of the matrix \hat{A} corresponds to the k th bond. In this paper, a system with N degrees of freedom and K bonds will be considered, which corresponds to $N \times K$ matrix \hat{A} . One can assume that the matrix elements A_{ik} are random due to the presence of disorder in the system. Therefore, the representation of the force-constant matrix in the form $\hat{\Phi} = \hat{A}\hat{A}^T$ corresponds to the Wishart ensemble of random matrices [30].

However, in real amorphous systems, different degrees of freedom and different bonds may be correlated with each other. Therefore, there is a nontrivial covariance matrix $C_{ij,kl} = \langle A_{ik} A_{jl} \rangle$ of the elements of the matrix \hat{A} (angular brackets denote the averaging over different realizations of the matrix \hat{A}). This leads to the study of the properties of the *correlated* Wishart ensemble.

Besides being correlated, the matrix \hat{A} has a certain structure. In real amorphous solids, short-range interaction between atoms dominates over long-range interaction. Therefore, the matrix \hat{A} and the force-constant matrix $\hat{\Phi}$ are naturally sparse matrices. The number and positions of nonzero elements in the matrix \hat{A} depend on the type of interaction between atoms in an amorphous solid. Each bond may involve several degrees of freedom, which affects the number of nonzero elements in the k th column of the matrix \hat{A} . For example, in the case of two-body potential (e.g., Lennard-Jones potential), each interaction involves six degrees of freedom. In the case of three-body potential (e.g., Stillinger-Weber potential [35]), each term, which depends on the covalent bond angle, involves nine degrees of freedom. Some interactions may also depend on the dihedral angle [36], which involves 12 degrees of freedom. Some of the individual interactions can be unstable without surrounding interactions of neighbor atoms. In this case, a linear combination of these interactions should be considered to make positive-definite bonds, which further increases the number of degrees of freedom under consideration. Thus, one can expect that the number of nonzero elements in each column of matrix \hat{A} is much greater than 1.

However, revealing the matrix \hat{A} and the covariance matrix \hat{C} for real amorphous systems is a complicated task, and the results obtained in this paper are based on general assumptions about the structure of these matrices. Since the force-constant matrix $\hat{\Phi}$ is invariant under the change of the sign of the matrix \hat{A} , the mean value of random elements A_{ik} is zero. In this paper, the matrix elements A_{ik} are assumed to be Gaussian random numbers with zero mean and covariance $C_{ij,kl}$. It is

worth noting that the absence of the matrix elements $A_{ik} = 0$ is equivalent to the absence of the corresponding matrix elements $C_{ii,kk} = 0$, so the case of the short-range interaction in a system corresponds to the sparse matrix \hat{C} . The above assumptions are taken into account in the correlated Wishart ensemble under consideration. The determination of the covariance matrix \hat{C} of an ensemble of disordered systems obtained by the molecular-dynamics simulations will be discussed in the following papers.

In this paper, we study the general properties of an amorphous system determined by the covariance matrix \hat{C} . The relation between \hat{C} and the effective force constant matrix $\hat{\Phi}^{\text{eff}}$ is obtained in Appendix A. This result is a generalization of the averaging method described in [37].

To describe the effective elastic properties of amorphous solids in the most simple form, it is further assumed that different bonds are uncorrelated with each other, but have different placements in space and involve different sets of degrees of freedom, which leads to the covariance in the following form:

$$\langle A_{ik}A_{jl} \rangle = C_{ij}^{(k)} \delta_{kl}. \quad (9)$$

In Ref. [32], a stronger assumption $\langle A_{ik}A_{jl} \rangle = C_{ij} \delta_{kl}$ was applied, which did not take into account that each column of the matrix \hat{A} may have its own covariance matrix, and could not be used to describe local elastic properties.

Using the results of Appendix A, the effective force-constant matrix can be presented as

$$\hat{\Phi}^{\text{eff}}(\omega^2) = \sum_k \gamma_k(\omega^2) \hat{C}^{(k)}, \quad (10)$$

where $\gamma_k(\omega^2)$ characterizes the frequency-dependent dimensionless stiffness of the k th bond and can be found from the following system of nonlinear equations:

$$\gamma_k(z) = 1 + \text{Tr} \left[\gamma_k(z) \hat{C}^{(k)} \left(\hat{m}z - \sum_l \gamma_l(z) \hat{C}^{(l)} \right)^{-1} \right], \quad (11)$$

where z is some complex number. In a general case, Eq. (11) can be solved numerically for any set of covariance matrices $\hat{C}^{(k)}$. However, in some cases Eq. (11) can be simplified, which is considered in the next section.

IV. EFFECTIVE ELASTIC MEDIUM

In this section, an amorphous solid with homogeneous statistical properties is considered. For such a medium, one can assume a homogeneous distribution of K bonds over a system with N degrees of freedom. In this case, one can introduce a smooth function $\gamma(\mathbf{r}, z)$ such that $\gamma_k(z) = \gamma(\mathbf{r}_k, z)$, where \mathbf{r}_k is a coordinate of the k th bond.

In the volume of a pure macroscopic amorphous solid, $\gamma(\mathbf{r}, z)$ does not depend on the coordinate \mathbf{r} . However, the boundary effects may lead to nonhomogeneous $\gamma(\mathbf{r}, z)$ near the boundaries of amorphous solids. In Appendix B, the differential equation for $\gamma(\mathbf{r}, z)$ is derived. In the static case ($z = \omega^2 = 0$), the equation for $\gamma(\mathbf{r}) \equiv \gamma(\mathbf{r}, 0)$ reads

$$(1 + \varkappa)\gamma(\mathbf{r}) = \varkappa + \xi_b^2 \nabla^2 \ln \gamma(\mathbf{r}), \quad (12)$$

where $\varkappa = K/N - 1$, ξ_b is a typical bond size, and ∇^2 denotes the Laplacian.

For slowly varying $\gamma(\mathbf{r})$ in the region near the point \mathbf{r} , the effective dynamical matrix has the form $\hat{\Phi}^{\text{eff}} = \gamma(\mathbf{r}) \langle \hat{\Phi} \rangle$, where $\langle \hat{\Phi} \rangle = \sum_k \hat{C}^{(k)}$ is the averaged force constant matrix. Therefore, $\gamma(\mathbf{r})$ can be considered as a dimensionless elasticity since elastic moduli of the reference medium described by $\langle \hat{\Phi} \rangle$ are multiplied by $\gamma(\mathbf{r})$.

Far from boundaries in an amorphous solid, $\gamma(\mathbf{r}) = \gamma_0 = \varkappa/(\varkappa + 1)$. If the number of random bonds is much greater than the number of degrees of freedom ($K \gg N$ and $\varkappa \gg 1$), self-averaging of random bonds takes place. It results in small fluctuations of the force constant matrix $\hat{\Phi}$. In this case, $\hat{\Phi}^{\text{eff}}$ is close to the average force constant matrix $\langle \hat{\Phi} \rangle$, and $\gamma_0 \approx 1$. The opposite case $\varkappa \ll 1$ corresponds to a strongly disordered solid with $\gamma_0 \ll 1$. Therefore, the effective medium is much softer than the reference medium described by the average force constant matrix $\langle \hat{\Phi} \rangle$. The role of disorder controlled by the parameter \varkappa on the vibrational properties of the bulk amorphous solid was studied in [32].

Equation (12) can be written as

$$\alpha(\mathbf{r}) = 1 + \xi^2 \nabla^2 \ln \alpha(\mathbf{r}), \quad (13)$$

where $\alpha(\mathbf{r}) = \gamma(\mathbf{r})/\gamma_0$ is the effective local elastic contrast, and $\xi = \xi_b/\sqrt{\varkappa}$ is the only dimensional parameter in the above equation.

The effective local elastic contrast $\alpha(\mathbf{r})$ specifies the effective local elastic moduli of the amorphous medium at coordinate \mathbf{r} : the local effective bulk modulus is $\mathcal{K}(\mathbf{r}) = \alpha(\mathbf{r})\mathcal{K}_0$ and the local effective shear modulus is $\mu(\mathbf{r}) = \alpha(\mathbf{r})\mu_0$, where \mathcal{K}_0 and μ_0 are the corresponding elastic moduli of a pure macroscopic amorphous solid. Near the boundaries, the effective local elastic contrast $\alpha(\mathbf{r})$ may differ from 1. The lengthscale of the boundary effects is described by ξ . Since $\xi \sim \varkappa^{-1/2}$, it depends on the strength of disorder. Therefore, ξ represents the heterogeneity lengthscale of the amorphous system. For a strongly disordered medium, $\xi \gg \xi_b$.

To obtain $\alpha(\mathbf{r})$ in the whole amorphous solid, Eq. (13) should be accomplished with the boundary conditions. The most important case is the interface of an amorphous medium with a more rigid and ordered medium. Such a rigid and ordered medium can be considered as a medium with $\varkappa \gtrsim 1$. In this case, one can assume $\gamma(\mathbf{r}) \sim 1$ on the boundaries. For a strongly disordered medium ($\varkappa \ll 1$), this boundary condition means $\alpha(\mathbf{r}) = \gamma(\mathbf{r})/\gamma_0 \sim 1/\varkappa \gg 1$. Therefore, without the loss of precision, one can assume that $\alpha(\mathbf{r}) = \infty$ on the boundaries to solve Eq. (13). Below, the two most important geometries of the boundary of an amorphous body are considered.

A. Flat boundary

Near a flat boundary, $\alpha(\mathbf{r})$ depends only on the distance from the boundary, which is denoted by x . In this case, Eq. (13) has the one-dimensional form

$$\alpha(x) = 1 + \xi^2 \frac{\partial^2}{\partial x^2} \ln \alpha(x). \quad (14)$$

The solution of Eq. (14) has a universal dependence on the scaled coordinate x/ξ , which is shown in Fig. 1. Far away

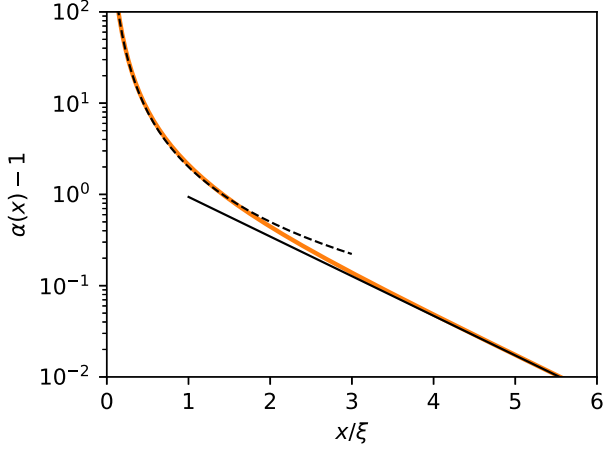


FIG. 1. The effective local elastic contrast $\alpha(x)$ near the flat boundary as a function of the scaled distance to the boundary. Solid and dashed black lines show the asymptotics given by Eqs. (15) and (16), respectively.

from the boundary ($x \gg \xi$), the asymptotic solution is

$$\alpha(x) = 1 + c_1 e^{-x/\xi}, \quad (15)$$

where $c_1 \approx 2.5527$. Near the boundary ($x \ll \xi$), the asymptotic solution is

$$\alpha(x) = \frac{2\xi^2}{x^2}. \quad (16)$$

One can note that solution (16) is inapplicable in the region $x \lesssim \xi_b$, where the assumption of the slow variation of $\alpha(x)$ on the lengthscale ξ_b is violated. Thus, the actual near-boundary value of $\alpha(x)$ is $\alpha(\xi_b) \sim 1/\nu$.

B. Spherical inclusion

Another important example is spherical nanoinclusions in an amorphous medium. Around each nanoinclusion, Eq. (13) can be written in spherical coordinates

$$\alpha(r) = 1 + \frac{\xi^2}{r^2} \frac{\partial}{\partial r} \left(r^2 \frac{\partial}{\partial r} \ln \alpha(r) \right), \quad (17)$$

where r is the distance from the center of the nanoinclusion of the radius R . The solution of Eq. (17) is shown in Fig. 2. Far away from the nanoinclusion ($r - R \gg \xi$), the asymptotic solution is

$$\alpha(r) = 1 + c_2 \frac{R}{r} e^{-(r-R)/\xi}, \quad (18)$$

where c_2 is a coefficient, which depends on the ratio R/ξ . The asymptotic solution near the surface of nanoinclusion ($r - R \ll \xi$, R) is

$$\alpha(r) = \frac{2R^2 \xi^2}{r^2 (r - R)^2}. \quad (19)$$

As in the one-dimensional case, solution (19) is inapplicable in a thin near-boundary region $r - R \lesssim \xi_b$. Thus, the actual near-boundary value of $\alpha(r)$ is $\alpha(R + \xi_b) \sim 1/\nu$.

Equations (18) and (19) show that the effective elastic shell is formed around the spherical nanoparticle. The typical thickness of this shell is about the heterogeneity lengthscale ξ .

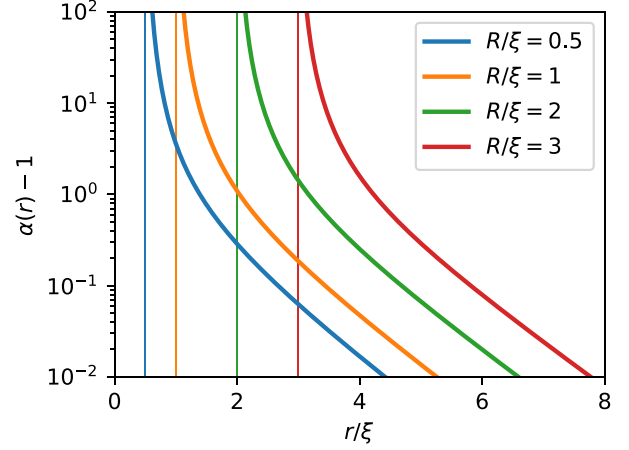


FIG. 2. The effective local elastic contrast $\alpha(r)$ around the spherical nanoinclusion as a function of the scaled distance from the center of the nanoparticle for different nanoparticle radii. Thin vertical lines mark the corresponding radius of the nanoparticle.

Thus, the presence of the nanoinclusion enhances the elastic properties at a distance ξ from the nanoparticle.

V. ELASTIC PROPERTIES OF A NANOCOMPOSITE

The macroscopic elastic properties of a nanocomposite describe a response (a strain) to macroscopic stress applied to the nanocomposite. For a nanocomposite with an amorphous host material, local strains exhibit large fluctuations. However, the macroscopic strain has negligible fluctuations. Therefore, as was shown in Sec. II, the macroscopic strain will be the same if the amorphous material is substituted with the effective elastic medium. Thus, the macroscopic elastic properties of a nanocomposite with amorphous host material can be found in two steps: (i) find the nonrandom continuous effective medium described by the local elastic contrast $\alpha(\mathbf{r})$, and (ii) find the macroscopic elastic properties of the nanocomposite with an effective medium using the classical elasticity theory.

A. Elasticity equations

The resulting spatial distribution of the effective local elastic contrast $\alpha(\mathbf{r})$ determines the local bulk and shear moduli of the effective medium as

$$\mathcal{K}(\mathbf{r}) = \alpha(\mathbf{r})\mathcal{K}_0, \quad (20)$$

$$\mu(\mathbf{r}) = \alpha(\mathbf{r})\mu_0. \quad (21)$$

Therefore, the relation between the local strain and stress tensors in the effective medium is determined by the usual elasticity equation

$$\sigma_{ij}(\mathbf{r}) = \mathcal{K}(\mathbf{r})\delta_{ij}\varepsilon_{kk}(\mathbf{r}) + 2\mu(\mathbf{r})(\varepsilon_{ij}(\mathbf{r}) - \frac{1}{3}\delta_{ij}\varepsilon_{kk}(\mathbf{r})). \quad (22)$$

In the stationary case, the stress tensor should satisfy the force balance equation

$$\frac{\partial}{\partial r_i} \sigma_{ij}(\mathbf{r}) = 0. \quad (23)$$

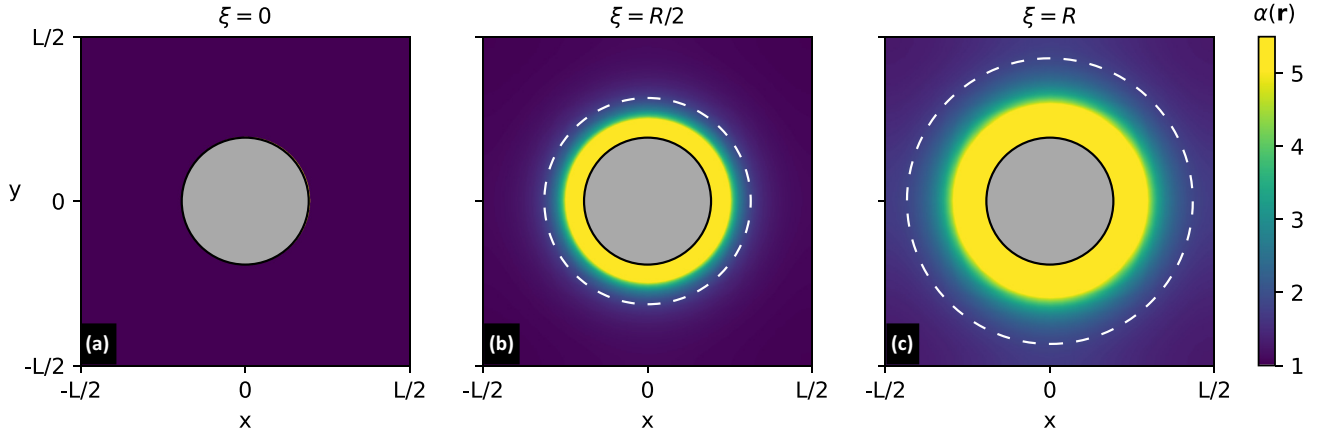


FIG. 3. The spatial distribution of the effective local elastic contrast $\alpha(\mathbf{r})$ for samples with different values of the heterogeneity lengthscale ξ . The section passing through the center of a spherical rigid inclusion of radius $R = 0.193L$ (indicated by the gray circle) is shown ($\phi = 3\%$). The white dashed line shows the circle of the radius $R + 1.25\xi$. The yellow color shows the area where the effective contrast $\alpha(\mathbf{r}) > 5$.

The macroscopic strain tensors $\varepsilon_{ij}^{\text{nc}}$ and stress tensors σ_{ij}^{nc} of a nanocomposite are a simple averaging over the composite volume of the corresponding local tensors:

$$\varepsilon_{ij}^{\text{nc}} = \overline{\varepsilon_{ij}(\mathbf{r})}, \quad (24)$$

$$\sigma_{ij}^{\text{nc}} = \overline{\sigma_{ij}(\mathbf{r})}. \quad (25)$$

The relationship between $\varepsilon_{ij}^{\text{nc}}$ and σ_{ij}^{nc} is determined by the macroscopic stiffness tensor of the nanocomposite $\mathcal{C}_{ijkl}^{\text{nc}}$ (not to be confused with the covariance matrix $C_{ij,kl}$):

$$\sigma_{ij}^{\text{nc}} = \mathcal{C}_{ijkl}^{\text{nc}} \varepsilon_{kl}^{\text{nc}}. \quad (26)$$

Thus, the general recipe for finding the macroscopic elastic moduli of a nanocomposite is to solve the system of equations (22)–(25) with some given deformation of the nanocomposite boundary. Comparing the set of macroscopic stresses σ_{ij}^{nc} and strains $\varepsilon_{ij}^{\text{nc}}$ for several trial deformations of the nanocomposite, all components of the macroscopic elasticity tensor $\mathcal{C}_{ijkl}^{\text{nc}}$ can be determined.

In many composite materials, the placement of inclusions is isotropic. In this case, the macroscopic elasticity tensor is defined by the macroscopic bulk modulus \mathcal{K}_{nc} and the macroscopic shear modulus μ_{nc} :

$$\mathcal{C}_{ijkl}^{\text{nc}} = \mathcal{K}_{\text{nc}} \delta_{ij} \delta_{kl} + \mu_{\text{nc}} (\delta_{ik} \delta_{jl} + \delta_{il} \delta_{jk} - \frac{2}{3} \delta_{ij} \delta_{kl}). \quad (27)$$

B. A numerical example

To demonstrate the proposed method, we present the numerical calculation of the elastic properties of a nanocomposite consisting of rigid spherical inclusions in the host amorphous matrix with some given heterogeneity lengthscale ξ . For simplicity of the calculation, the inclusions are placed in sites of a simple-cubic lattice with period L . In this case, Eq. (13) can be solved in one periodic cubic cell $L \times L \times L$ with one rigid spherical inclusion of radius R placed in the center of the cell.

The finite-element method with the hexahedral mesh is used, which was described in detail in [38]. The mesh containing 303 104 elements is considered to achieve enough numerical precision. FEniCS v0.5.2 [39] is used to solve the finite-element problem using variational formulation.

The effective local elastic contrast $\alpha(\mathbf{r})$ is found using Eq. (13) on the mesh under consideration. Figure 3 shows the obtained spatial distribution of effective local elastic contrast $\alpha(\mathbf{r})$ for different heterogeneity lengthscale ξ in the plane passing through the center of the inclusion of radius $R = 0.193L$. The corresponding volume fraction of inclusions is $\phi = \frac{4}{3} \pi R^3 / L^3 = 3\%$. For an amorphous matrix, Poisson's ratio was chosen as $\nu_0 = 0.3$, which is a typical value for amorphous polymers. Figure 3 shows a reinforced shell with $\alpha(\mathbf{r}) \gg 1$ with the thickness of the order of ξ around the nanoparticle.

To solve elasticity equations for a composite with periodic boundary conditions under consideration, the boundary conditions can be satisfied by considering the displacement in the form

$$u_i(\mathbf{r}) = \varepsilon_{ij}^{\text{nc}} r_j + \tilde{u}_i(\mathbf{r}), \quad (28)$$

where $\tilde{u}_i(\mathbf{r})$ is a periodic function

$$\begin{aligned} \tilde{u}_i(x, y, z) &= \tilde{u}_i(x + L, y, z) = \tilde{u}_i(x, y + L, z) \\ &= \tilde{u}_i(x, y, z + L). \end{aligned} \quad (29)$$

The resulting strain tensor is given by

$$\varepsilon_{ij}(\mathbf{r}) = \varepsilon_{ij}^{\text{nc}} + \frac{1}{2} \left(\frac{\partial \tilde{u}_i(\mathbf{r})}{\partial r_j} + \frac{\partial \tilde{u}_j(\mathbf{r})}{\partial r_i} \right). \quad (30)$$

Elasticity equations (22) and (23) with boundary conditions (29) were solved using the finite-element method with the same numerical mesh. Samples with the fixed inclusion volume fraction $\phi = 3\%$ and different values of the lengthscale ξ were analyzed. Then the average stress σ_{ij}^{nc} was calculated by Eq. (25) for volumetric and shear deformations of the nanocomposite given by the corresponding strain tensor $\varepsilon_{ij}^{\text{nc}}$. The resulting bulk modulus \mathcal{K}_{nc} and shear modulus μ_{nc} were obtained by Eqs. (26) and (27). For the small volume fraction of inclusions under consideration, the cubic anisotropy of the composite due to the periodic arrangement of the inclusions can be neglected.

Figure 4 shows the results of calculating the reinforcement of an amorphous medium due to spherical rigid inclusions

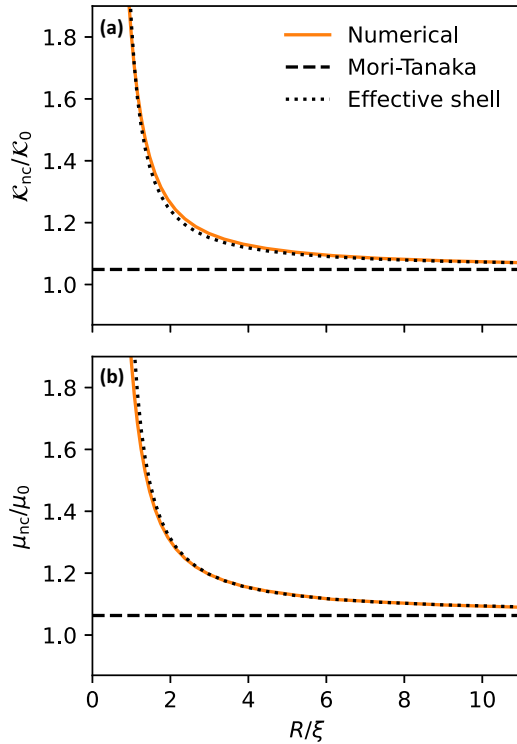


FIG. 4. The ratio of the nanocomposite elastic moduli to the corresponding moduli of the host amorphous medium depending on the ratio R/ξ for the given volume fraction of rigid spherical inclusions $\phi = 3\%$. Solid lines are the result of numerical simulation, horizontal dashed lines are the Mori-Tanaka model for rigid inclusions with radius R , and dotted lines are the modified Mori-Tanaka model for rigid inclusions with effective inclusion radius $R^{\text{eff}} = R + 1.25\xi$.

with the fixed inclusion volume fraction $\phi = 3\%$ and different ratios R/ξ .

For homogeneous host material without disorder ($\xi = 0$), the macroscopic stiffness of the nanocomposite can be calculated using the Mori-Tanaka theory [40,41]. The addition of a small concentration of rigid spherical inclusions to the host material leads to the following macroscopic elastic moduli of the nanocomposite:

$$\mathcal{K}_{\text{MT}} = \mathcal{K}_0 \left(1 + 3\phi \frac{1 - \nu_0}{1 + \nu_0} \right), \quad (31)$$

$$\mu_{\text{MT}} = \mu_0 \left(1 + \frac{15\phi}{2} \frac{1 - \nu_0}{4 - 5\nu_0} \right). \quad (32)$$

For $\phi = 3\%$, Eqs. (31) and (32) predict the increase of the bulk modulus by 4.8% and the shear modulus by 6.3% due to the presence of inclusions. These values are shown in Fig. 4 by horizontal dashed lines since they do not depend on the heterogeneity lengthscale ξ .

For amorphous host material with $\xi \sim R$ (see solid lines in Fig. 4), the macroscopic elastic moduli \mathcal{K}_{nc} and μ_{nc} of nanocomposite are significantly larger than the prediction by the Mori-Tanaka theory. For $\xi \ll R$, the macroscopic elastic moduli approach the values given by the Mori-Tanaka theory.

To understand this behavior, the effective shell with enhanced elastic properties around inclusions (Fig. 3) should be taken into account. The thickness of this shell is

approximately the heterogeneity lengthscale ξ , which can increase the effective radius of the inclusions by a value of the order of ξ . Therefore, we plot the additional dotted lines in Fig. 4 with the Mori-Tanaka theory but with increased nanoparticle radius $R^{\text{eff}} = R + 1.25\xi$. One can see a good agreement with a such modification of the existing theory. The numerical factor was chosen for better fitting of the result. The effective shell of the thickness 1.25ξ is shown in Fig. 4 by dashed circles for a visual guide. A typical value of the local elastic contrast is $\alpha(\mathbf{r}) \approx 1.8$ at this distance from the inclusion. Thus, the amorphous medium in the effective shell has much higher rigidity than the amorphous medium far from inclusion.

The obtained elastic properties of nanocomposites can be described quantitatively by the three-phase model [21]. However, it is important that the effective interphase shell can be formed solely due to the disorder without any structural change of the amorphous medium near the inclusion.

VI. DISCUSSION

The obtained effective force constant matrix $\hat{\Phi}^{\text{eff}}$ can be used as a nonrandom substitution of the random force constant matrix $\hat{\Phi}$, which gives the same average response to external forces. In particular, $\hat{\Phi}^{\text{eff}}$ can be used to represent the macroscopic elastic properties of composite materials containing amorphous materials.

Using the random matrix theory, the effective force constant matrix $\hat{\Phi}^{\text{eff}}$ was obtained. In the continuum limit, amorphous solids with homogeneous and isotropic statistics are described by the local elastic contrast $\alpha(\mathbf{r})$ given by Eq. (13). This is the main equation of the present work, which contains only the heterogeneity lengthscale ξ . This lengthscale is the main parameter of the amorphous medium, which appears to be important in the given study. Near the boundary with a more rigid medium, the local elastic contrast $\alpha(\mathbf{r}) \gg 1$. The thickness of such a boundary layer with increased stiffness is of the order of the heterogeneity lengthscale ξ .

The results of this work are not limited to amorphous solids. They can be extended to any systems with strongly disordered elastic properties (e.g., granular systems), where ξ can be treated as a phenomenological parameter, which describes the heterogeneity lengthscale of the system.

The studied effect is especially important for nanocomposites with an amorphous host material. In this case, one can find the macroscopic elastic moduli in two steps: (i) find the effective local elastic contrast $\alpha(\mathbf{r})$, and (ii) use classical elasticity theory to find macroscopic elastic properties of the nanocomposite with the effective continuous medium. An example of this approach was presented in Sec. VB. The disorder of the host material leads to the formation of an effective shell of thickness ξ with increased stiffness around each nanoparticle. In this case, the nanoparticles have an effective radius R_{eff} such that $R_{\text{eff}} - R \sim \xi$. Thus, for $R \sim \xi$ the influence of nanoinclusions on the macroscopic stiffness of the nanocomposite will be increased by an order of magnitude.

Figure 4 shows the dependence of the reinforcement on the inclusion size. The experimental results have shown a similar dependence [42], which means the presence of an effective interphase shell around inclusions. However, determining

whether the shell is due to the inhomogeneity lengthscale or structural changes in the matrix near the inclusion requires additional study for each given composite material.

The main result (13) concerns the static stiffness; however, Eqs. (11) and (B6) may be applied to arbitrary frequency ω given by the parameter $z = \omega^2$. For amorphous solids with homogeneous and isotropic statistics, far away from boundaries, $\gamma_k(z)$ does not depend on k and can be written as $\gamma_k(z) = z/Z(z)$, where $Z(z)$ is some complex function. In this case, $\hat{\Phi}^{\text{eff}}(z) = \frac{z}{Z(z)} \sum_k \hat{C}^{(k)} = \frac{z}{Z(z)} \langle \hat{M} \rangle$. Therefore, summing Eq. (11) over k , we obtain the complex equation

$$\varkappa Z(z) + \frac{Z(z)^2}{N} \text{Tr} \left[\frac{1}{Z(z) - \langle \hat{M} \rangle} \right] = (1 + \varkappa)z, \quad (33)$$

where $\langle \hat{M} \rangle = \hat{m}^{-1/2} \langle \hat{\Phi} \rangle \hat{m}^{-1/2}$ is the average dynamical matrix. For any given $z = \omega^2 - i0$, one can find $Z(z)$ and obtain the vibrational density of states $g(\omega) = (1 + \varkappa) \frac{2\pi}{\omega} \text{Im}[1/Z(\omega^2 - i0)]$. A more detailed analysis of vibrational properties has been done in [32].

Amorphous solids have an excess of low-frequency vibrational density of states, known as the boson peak [43,44]. The boson peak lengthscale defined as $\xi_{\text{bp}} = 2\pi c_T / \omega_{\text{bp}}$, where c_T is the transverse sound velocity and ω_{bp} is the boson peak frequency, was attributed to the heterogeneity lengthscale [10]. In the random matrix model, the boson peak lengthscale is $\xi_{\text{bp}} \sim a_0 \varkappa^{-1/2}$, where a_0 is the interatomic distance [32]. Thus, the heterogeneity lengthscales ξ and ξ_{bp} have the same order and the same dependence on the strength of disorder in the studied random matrix model.

In real amorphous solids, the strength of disorder cannot be varied in a wide range. However, model granular systems, known as jammed solids, have the possibility to change their properties significantly [45]. This is due to a critical behavior of the elastic and vibrational properties for small positive values of the parameter $z - z_0$ [46–48], which corresponds to the parameter \varkappa in the present theory [32]. In jammed solids, the lengthscale $l_c \sim (z - z_c)^{-1/2}$ is related to the breakdown of the continuum elasticity [49] and coincides with the boson peak lengthscale [46]. Thus, the lengthscale l_c corresponds to the lengthscale ξ in the present theory. The investigation of the local elastic properties near the boundaries of jammed solids is of great interest to check the validity of Eq. (13) for such systems.

The obtained results are not limited to the study of the elastic properties of strongly disordered systems. Other properties requiring positive-definiteness can be considered. For example, instead of stiffness, one can consider the conductivity of a strongly disordered medium. Thus, $\alpha(\mathbf{r})$ can describe the increase of the conductivity of the effective medium near the interface with a well-conducting material. The applicability of the considered model to such systems will be the subject of further research.

VII. CONCLUSION

In this paper, the theory of correlated random matrices was applied to find the local elastic properties of amorphous solids. The effective force constant matrix $\hat{\Phi}^{\text{eff}}(z)$ was obtained,

which can be used to find the average linear response to a force of a given frequency ω given by the parameter $z = \omega^2$.

For amorphous solids with homogeneous and isotropic statistical properties, a continuous equation for effective local elastic contrast $\alpha(\mathbf{r})$ was obtained. This equation shows the increase of the stiffness of the amorphous solid near the boundary with a more rigid and ordered body. The typical thickness of the boundary layer with increased stiffness is the heterogeneity lengthscale ξ . Far away from the boundaries, $\alpha(\mathbf{r})$ has an exponential decay to 1 with a typical length ξ .

For the strongly disordered amorphous solids, the heterogeneity lengthscale ξ is much larger than the typical interatomic size in the system. The scaling of ξ with the strength of disorder emphasizes the role of disorder in the formation of the boundary layer with increased stiffness.

The effect under study is important for macroscopic elastic moduli of nanocomposites with the amorphous host material. The numerical model of an amorphous solid with rigid spherical inclusions was studied to demonstrate the effect. It was shown that a shell with enhanced elastic properties is formed around each nanoparticle. The thickness of this shell is of the order of ξ , which results in the increased effective radius of nanoparticles, which significantly increases the macroscopic elastic moduli of the nanocomposite.

ACKNOWLEDGMENT

The financial support from Russian Science Foundation under Grant No. 22-72-10083 is gratefully acknowledged. The authors thank A. V. Shumilin for the valuable discussions.

APPENDIX A: RANDOM MATRIX THEORY: THE AVERAGING PROCEDURE

The averaging in the resolvent $G(z) = \langle (\hat{m}z - \hat{\Phi})^{-1} \rangle$ can be done analytically for $\hat{\Phi} = \hat{A}\hat{A}^T$ in the assumption that the \hat{A} is a Gaussian random matrix with zero mean and the covariance of matrix elements $\langle A_{ik}A_{jl} \rangle = C_{ij,kl}$. The resolvent $G(z)$ can be presented as an infinite series

$$\begin{aligned} \hat{G}(z) &= \left\langle \frac{1}{\hat{m}z - \hat{A}\hat{A}^T} \right\rangle = \frac{1}{\hat{m}z} + \left\langle \frac{1}{\hat{m}z} \hat{A}\hat{A}^T \frac{1}{\hat{m}z} \right\rangle \\ &+ \left\langle \frac{1}{\hat{m}z} \hat{A}\hat{A}^T \frac{1}{\hat{m}z} \hat{A}\hat{A}^T \frac{1}{\hat{m}z} \right\rangle + \dots \end{aligned} \quad (A1)$$

The elements of the resolvent $\hat{G}(z)$ can be written explicitly in the following form:

$$\begin{aligned} G_{ij}(z) &= (\hat{m}z)_{ij}^{-1} + \sum_{i_1 k_1 i_2 k_2} (\hat{m}z)_{i_1 i_1}^{-1} \delta_{k_1 k_2} (\hat{m}z)_{i_2 j}^{-1} \langle A_{i_1 k_1} A_{i_2 k_2} \rangle \\ &+ \sum_{i_1 k_1 i_2 k_2 i_3 k_3 i_4 k_4} (\hat{m}z)_{i_1 i_1}^{-1} \delta_{k_1 k_2} (\hat{m}z)_{i_2 i_3}^{-1} \delta_{k_3 k_4} (\hat{m}z)_{i_4 j}^{-1} \\ &\times \langle A_{i_1 k_1} A_{i_2 k_2} A_{i_3 k_3} A_{i_4 k_4} \rangle + \dots \end{aligned} \quad (A2)$$

We follow from the diagram technique described in [37] and introduce the next graphical representation:

$$(\hat{m}z)_{ij}^{-1} = \text{---} \overset{i}{\bullet} \text{---} \overset{j}{\bullet} \text{---}, \quad \delta_{kl} = \overset{k}{\circ} \text{---} \overset{l}{\circ}, \quad \langle A_{ik}A_{jl} \rangle = C_{ij,kl} = \text{---} \overset{i}{\bullet} \text{---} \overset{k}{\circ} \text{---} \overset{l}{\circ} \text{---} \overset{j}{\bullet} \text{---}$$

Here the solid line joining i and j is the factor $(\hat{m}z)_{ij}^{-1}$, the dashed line joining k and l is the Kronecker symbol δ_{kl} , and a double arc joining i, k and l, j is the propagator $C_{ij,kl}$. Following these rules, the second term in (A2) corresponds to

$$\begin{aligned} \langle A_{i_1 k_1} A_{i_2 k_2} A_{i_3 k_3} A_{i_4 k_4} \rangle &= \langle A_{i_1 k_1} A_{i_2 k_2} \rangle \langle A_{i_3 k_3} A_{i_4 k_4} \rangle + \langle A_{i_1 k_1} A_{i_4 k_4} \rangle \langle A_{i_2 k_2} A_{i_3 k_3} \rangle + \langle A_{i_1 k_1} A_{i_3 k_3} \rangle \langle A_{i_2 k_2} A_{i_4 k_4} \rangle \\ &= \text{---} \overset{i_1}{\bullet} \text{---} \overset{k_1}{\circ} \text{---} \overset{i_2}{\bullet} \text{---} \overset{k_2}{\circ} \text{---} + \text{---} \overset{i_1}{\bullet} \text{---} \overset{k_2}{\circ} \text{---} \overset{i_3}{\bullet} \text{---} \overset{k_3}{\circ} \text{---} + \text{---} \overset{i_1}{\bullet} \text{---} \overset{k_2}{\circ} \text{---} \overset{i_3}{\bullet} \text{---} \overset{k_4}{\circ} \text{---} \end{aligned}$$

Therefore, a graphical representation of the resolvent $\hat{G}(z)$ is

$$\text{---} \overset{G}{\bullet} \text{---} = \text{---} \overset{\bullet}{\bullet} \text{---} + \text{---} \overset{\bullet}{\circ} \text{---} \overset{\circ}{\bullet} \text{---} + \text{---} \overset{\bullet}{\circ} \text{---} \overset{\circ}{\bullet} \text{---} \overset{\bullet}{\circ} \text{---} \overset{\circ}{\bullet} \text{---} + \text{---} \overset{\bullet}{\circ} \text{---} \overset{\circ}{\bullet} \text{---} \overset{\bullet}{\circ} \text{---} \overset{\circ}{\bullet} \text{---} \overset{\bullet}{\circ} \text{---} \overset{\circ}{\bullet} \text{---} + \dots \tag{A3}$$

The presentation (A3) allows us to distinguish planar and nonplanar diagrams. For planar diagrams, the number of closed loops (closed solid line or closed dashed line) is equal to the number of double arcs. For nonplanar diagrams, the number of closed loops is less than the number of double arcs. Namely, the second diagram in (A3) is planar and contains one closed loop and one double arc, the third and fourth diagrams are planar and contain two closed loops and two double arcs, and the fifth diagram is nonplanar and contains two double arcs and only one closed loop.

Each closed loop \mathcal{L} corresponds to the calculation of a trace, which gives some factor $T_{\mathcal{L}}$ depending on the number of nonzero elements of the matrix \hat{C} . If each bond involves a sufficiently large number of degrees of freedom (although the matrix \hat{C} can be a highly sparse matrix), the factor $T_{\mathcal{L}} \gg 1$ for each closed loop \mathcal{L} . In the case of a sufficiently filled matrix \hat{C} , the factor $T_{\mathcal{L}} \sim N$. At the condition $T_{\mathcal{L}} \gg 1$, each planar diagram contributes much more than a nonplanar diagram with the same number of double arcs. Therefore, we can exclude nonplanar diagrams from the summation (A3) and take into account only planar diagrams.

One can draw $\hat{G}(z)$ using the self-energy $\hat{\Sigma}(z)$, which contains only planar diagrams:

$$\text{---} \overset{G}{\bullet} \text{---} = \text{---} \overset{\bullet}{\bullet} \text{---} + \text{---} \overset{\Sigma}{\bullet} \text{---} + \text{---} \overset{\Sigma}{\bullet} \text{---} \overset{\Sigma}{\bullet} \text{---} + \dots \tag{A4}$$

The matrix $\hat{\Sigma}(z)$ can be expressed using the other resolvent $\hat{G}^*(z) = \langle (1 - \hat{A}^T (\hat{m}z)^{-1} \hat{A})^{-1} \rangle$ by the Dyson-Schwinger relation:

$$\text{---} \overset{\Sigma}{\bullet} \text{---} = \text{---} \overset{G^*}{\bullet} \text{---} \tag{A5}$$

The resolvent $\hat{G}^*(z)$ contains all diagrams of the same shape as in (A3) with dashed and solid lines replaced. Therefore,

the next diagram:

$$\sum_{i_1 k_1 i_2 k_2} (\hat{m}z)_{i_1 i_1}^{-1} \delta_{k_1 k_2} (\hat{m}z)_{i_2 i_2}^{-1} \langle A_{i_1 k_1} A_{i_2 k_2} \rangle = \text{---} \overset{i}{\bullet} \text{---} \overset{k_1}{\circ} \text{---} \overset{k_2}{\circ} \text{---} \overset{j}{\bullet} \text{---}$$

Since the elements of the matrix \hat{A} are Gaussian random numbers, Wick's probability theorem is applicable for consecutively calculating even-point correlation functions, which are expressed as sums of all distinct products of two-point functions $\langle A_{i_1 k_1} A_{i_2 k_2} \rangle$:

analogously to Eq. (A4), it can be written as

$$\text{---} \overset{G^*}{\bullet} \text{---} = \text{---} \overset{\circ}{\circ} \text{---} + \text{---} \overset{\Sigma^*}{\circ} \text{---} + \text{---} \overset{\Sigma^*}{\circ} \text{---} \overset{\Sigma^*}{\circ} \text{---} + \dots \tag{A6}$$

where the self-energy $\hat{\Sigma}^*(z)$ is related to $\hat{G}(z)$ by the Dyson-Schwinger relation:

$$\text{---} \overset{\Sigma^*}{\circ} \text{---} = \text{---} \overset{G}{\bullet} \text{---} \tag{A7}$$

As a result, we obtain the closed set of four equations that correspond to the graphical representation (A4)–(A7):

$$\hat{G}(z) = \frac{1}{\hat{m}z - \hat{\Sigma}(z)}, \quad \Sigma_{ij}(z) = \sum_{kl} C_{ij,kl} G_{kl}^*(z), \tag{A8}$$

$$\hat{G}^*(z) = \frac{1}{1 - \hat{\Sigma}^*(z)}, \quad \Sigma_{kl}^*(z) = \sum_{ij} C_{ij,kl} G_{ij}(z). \tag{A9}$$

As follows from Eq. (6), the matrix $\hat{\Sigma}(z)$ plays the role of an effective force-constant matrix $\hat{\Phi}^{\text{eff}}(z)$ describing the properties of an effective medium:

$$\Phi_{ij}^{\text{eff}}(z) = \Sigma_{ij}(z). \tag{A10}$$

For any given covariance matrix $C_{ij,kl}$, one can solve Eqs. (A8) and (A9) and find the effective force-constant matrix $\hat{\Phi}^{\text{eff}}(z)$.

In the case of uncorrelated bonds, the matrix elements A_{ik} and A_{jl} are independent for $k \neq l$. The corresponding covariance matrix is

$$C_{ij,kl} = C_{ij}^{(k)} \delta_{kl}. \tag{A11}$$

In this case, $\hat{G}^*(z)$ has a diagonal form, $G_{kl}^*(z) = \gamma_k(z)\delta_{kl}$, and the solution of Eqs. (A8)–(A9) can be presented in the following simplified form:

$$\Phi_{ij}^{\text{eff}}(z) = \sum_k C_{ij}^{(k)} \gamma_k(z), \quad (\text{A12})$$

$$\gamma_k(z) = 1 + \text{Tr} \left[\gamma_k(z) \hat{C}^{(k)} \left(\hat{m}z - \sum_l \gamma_l(z) \hat{C}^{(l)} \right)^{-1} \right]. \quad (\text{A13})$$

APPENDIX B: AMORPHOUS SOLID WITH HOMOGENEOUS AND ISOTROPIC STATISTICAL PROPERTIES

One can assume that $\gamma_l(z) = \gamma(\mathbf{r}_l, z)$ is close to $\gamma_k(z) = \gamma(\mathbf{r}_k, z)$ for neighbor bonds k and l . In this case, Eq. (11) can be written as

$$\begin{aligned} \gamma_k(z) = 1 + W_k(Z) + \sum_l W_{kl}(Z) \frac{\gamma_l(z) - \gamma_k(z)}{\gamma_k(z)} \\ + \sum_{lm} W_{klm}(Z) \frac{[\gamma_l(z) - \gamma_k(z)][\gamma_m(z) - \gamma_k(z)]}{\gamma_k^2(z)}, \end{aligned} \quad (\text{B1})$$

where $Z = z/\gamma_k(z)$ and

$$W_k(Z) = \text{Tr} \left[\hat{C}^{(k)} \frac{1}{\hat{m}Z - \langle \hat{\Phi} \rangle} \right], \quad (\text{B2})$$

$$W_{kl}(Z) = \text{Tr} \left[\hat{C}^{(k)} \frac{1}{\hat{m}Z - \langle \hat{\Phi} \rangle} \hat{C}^{(l)} \frac{1}{\hat{m}Z - \langle \hat{\Phi} \rangle} \right], \quad (\text{B3})$$

$$\begin{aligned} W_{klm}(Z) = \text{Tr} \left[\hat{C}^{(k)} \frac{1}{\hat{m}Z - \langle \hat{\Phi} \rangle} \hat{C}^{(l)} \frac{1}{\hat{m}Z - \langle \hat{\Phi} \rangle} \hat{C}^{(m)} \right. \\ \left. \times \frac{1}{\hat{m}Z - \langle \hat{\Phi} \rangle} \right]. \end{aligned} \quad (\text{B4})$$

At the same time, $\gamma_l(z) - \gamma_k(z)$ can be written as

$$\begin{aligned} \gamma_l(z) - \gamma_k(z) = \sum_{\alpha} \frac{\partial \gamma(\mathbf{r}_k, z)}{\partial r_{\alpha}} (r_{l\alpha} - r_{k\alpha}) \\ + \frac{1}{2} \sum_{\alpha\beta} \frac{\partial^2 \gamma(\mathbf{r}_k, z)}{\partial r_{\alpha} \partial r_{\beta}} (r_{l\alpha} - r_{k\alpha})(r_{l\beta} - r_{k\beta}). \end{aligned} \quad (\text{B5})$$

As a result, the following differential equation for $\gamma(\mathbf{r}, z)$ is obtained:

$$\begin{aligned} \gamma(\mathbf{r}, z) = 1 + W(\mathbf{r}, Z) + \frac{1}{\gamma(\mathbf{r}, z)} \sum_{\alpha} W'_{\alpha}(\mathbf{r}, Z) \frac{\partial \gamma(\mathbf{r}, z)}{\partial r_{\alpha}} \\ + \frac{1}{\gamma(\mathbf{r}, z)} \sum_{\alpha\beta} W'_{\alpha\beta}(\mathbf{r}, Z) \frac{\partial^2 \gamma(\mathbf{r}, z)}{\partial r_{\alpha} \partial r_{\beta}} \\ + \frac{1}{\gamma(\mathbf{r}, z)^2} \sum_{\alpha\beta} W''_{\alpha\beta}(\mathbf{r}, Z) \frac{\partial \gamma(\mathbf{r}, z)}{\partial r_{\alpha}} \frac{\partial \gamma(\mathbf{r}, z)}{\partial r_{\beta}}, \end{aligned} \quad (\text{B6})$$

where

$$W(\mathbf{r}_k, Z) = W_k(Z), \quad (\text{B7})$$

$$W'_{\alpha}(\mathbf{r}_k, Z) = \sum_l W_{kl}(Z)(r_{l\alpha} - r_{k\alpha}), \quad (\text{B8})$$

$$W'_{\alpha\beta}(\mathbf{r}_k, Z) = \frac{1}{2} \sum_l W_{kl}(Z)(r_{l\alpha} - r_{k\alpha})(r_{l\beta} - r_{k\beta}), \quad (\text{B9})$$

$$W''_{\alpha\beta}(\mathbf{r}_k, Z) = \sum_{lm} W_{klm}(Z)(r_{l\alpha} - r_{k\alpha})(r_{m\beta} - r_{k\beta}). \quad (\text{B10})$$

Static properties are defined by the limit $z \rightarrow 0$ and $Z \rightarrow 0$. In this case, there are the following sum rules:

$$\sum_k W_k(0) = N_0 - N, \quad (\text{B11})$$

$$\sum_l W_{kl}(0) = -W_k(0), \quad (\text{B12})$$

$$\sum_m W_{klm}(0) = -W_{kl}(0), \quad (\text{B13})$$

where N_0 is the number of trivial zero-frequency modes (translations and rotations), which can be neglected for $N \gg 1$. Using Eqs. (B11)–(B13), for an amorphous solid with homogeneous and isotropic statistical properties, one obtains

$$W(\mathbf{r}_k, 0) = -\frac{N}{K}, \quad (\text{B14})$$

$$W'_{\alpha}(\mathbf{r}_k, 0) = 0, \quad (\text{B15})$$

$$W'_{\alpha\beta}(\mathbf{r}_k, 0) = \frac{N}{K} \xi_b^2 \delta_{\alpha\beta}, \quad (\text{B16})$$

$$W''_{\alpha\beta}(\mathbf{r}_k, 0) = -\frac{N}{K} \xi_b^2 \delta_{\alpha\beta}, \quad (\text{B17})$$

where ξ_b is a typical radius of the bonds. As a result, in the static case ($z = 0$) we obtain

$$\gamma(\mathbf{r}, 0) = 1 - \frac{N}{K} + \frac{N}{K} \xi_b^2 \nabla^2 \ln \gamma(\mathbf{r}, 0). \quad (\text{B18})$$

- [1] K. Yoshimoto, T. S. Jain, K. Van Workum, P. F. Nealey, and J. J. de Pablo, *Phys. Rev. Lett.* **93**, 175501 (2004).
 [2] M. Tsamados, A. Tanguy, C. Goldenberg, and J.-L. Barrat, *Phys. Rev. E* **80**, 026112 (2009).
 [3] H. Wagner, D. Bedorf, S. Kuechemann, M. Schwabe, B. Zhang, W. Arnold, and K. Samwer, *Nat. Mater.* **10**, 439 (2011).

- [4] H. Mizuno, S. Mossa, and J.-L. Barrat, *Phys. Rev. E* **87**, 042306 (2013).
 [5] R. Jana and L. Pastewka, *J. Phys.: Mater.* **2**, 045006 (2019).
 [6] Q. Wen, A. Basu, P. A. Janmey, and A. G. Yodh, *Soft Matter* **8**, 8039 (2012).

- [7] E. Del Gado, P. Ilg, M. Kröger, and H. C. Öttinger, *Phys. Rev. Lett.* **101**, 095501 (2008).
- [8] C. Goldenberg, A. Tanguy, and J.-L. Barrat, *Europhys. Lett.* **80**, 16003 (2007).
- [9] F. Leonforte, A. Tanguy, J. P. Wittmer, and J.-L. Barrat, *Phys. Rev. Lett.* **97**, 055501 (2006).
- [10] F. Leonforte, R. Boissière, A. Tanguy, J. P. Wittmer, and J.-L. Barrat, *Phys. Rev. B* **72**, 224206 (2005).
- [11] A. Tanguy, J. P. Wittmer, F. Leonforte, and J.-L. Barrat, *Phys. Rev. B* **66**, 174205 (2002).
- [12] Y. W. Mai and Z. Z. Yu, *Polymer Nanocomposites*, Woodhead Publishing Series in Composites Science and Engineering (Elsevier Science, Cambridge, 2006).
- [13] E. T. Thostenson and T.-W. Chou, *J. Phys. D* **36**, 573 (2003).
- [14] M. A. Rafiee, J. Rafiee, Z. Wang, H. Song, Z.-Z. Yu, and N. Koratkar, *ACS Nano* **3**, 3884 (2009).
- [15] A. Mesbah, F. Zaïri, S. Boutaleb, J.-M. Gloaguen, M. Naït-Abdelaziz, S. Xie, T. Boukharouba, and J.-M. Lefebvre, *J. Appl. Polym. Sci.* **114**, 3274 (2009).
- [16] S.-Y. Fu, X.-Q. Feng, B. Lauke, and Y.-W. Mai, *Composites Part B: Eng.* **39**, 933 (2008).
- [17] Y. Ou, F. Yang, and Z.-Z. Yu, *J. Polym. Sci. Pt. B* **36**, 789 (1998).
- [18] H. Wang, Y. Bai, S. Liu, J. Wu, and C. P. Wong, *Acta Mater.* **50**, 4369 (2002).
- [19] B. Wetzal, F. Hauptert, and M. Q. Zhang, *Compos. Sci. Technol.* **63**, 2055 (2003).
- [20] V. A. Bershtein, O. P. Grigoryeva, P. N. Yakushev, and A. M. Fainleib, *Polym. Compos.* **42**, 6777 (2021).
- [21] G. M. Odegard, T. C. Clancy, and T. S. Gates, *Polymer* **46**, 553 (2005).
- [22] F. Bondioli, V. Cannillo, E. Fabbri, and M. Messori, *J. Appl. Polym. Sci.* **97**, 2382 (2005).
- [23] S. Saber-Samandari and A. Afaghi-Khatibi, *Polym. Compos.* **28**, 405 (2007).
- [24] R. Qiao and L. C. Brinson, *Compos. Sci. Technol.* **69**, 491 (2009).
- [25] H. W. Wang, H. W. Zhou, R. D. Peng, and L. Mishnaevsky Jr, *Compos. Sci. Technol.* **71**, 980 (2011).
- [26] J. Amraei, J. E. Jam, B. Arab, and R. D. Firouz-Abadi, *J. Compos. Mater.* **53**, 1261 (2019).
- [27] M. Bazmara, M. Silani, and I. Dayyani, *Defence Technol.* **17**, 177 (2021).
- [28] J. Fankhänel, B. Arash, and R. Rolfes, *Composites Pt. B: Eng.* **176**, 107211 (2019).
- [29] Y. M. Beltukov, D. A. Conyuh, and I. A. Solov'yov, *Phys. Rev. E* **105**, L012501 (2022).
- [30] Y. M. Beltukov, V. I. Kozub, and D. A. Parshin, *Phys. Rev. B* **87**, 134203 (2013).
- [31] D. A. Conyuh, Y. M. Beltukov, and D. A. Parshin, *Phys. Solid State* **61**, 1272 (2019).
- [32] D. A. Conyuh and Y. M. Beltukov, *Phys. Rev. B* **103**, 104204 (2021).
- [33] R. Bhatia, *Positive Definite Matrices* (Princeton University Press, Princeton, NJ, 2009).
- [34] Y. M. Beltukov and D. A. Parshin, *JETP Lett.* **104**, 552 (2016).
- [35] F. H. Stillinger and T. A. Weber, *Phys. Rev. B* **31**, 5262 (1985).
- [36] S. L. Mayo, B. D. Olafson, and W. A. Goddard, *J. Phys. Chem.* **94**, 8897 (1990).
- [37] Z. Burda, A. Görlich, A. Jarosz, and J. Jurkiewicz, *Physica A* **343**, 295 (2004).
- [38] A. A. Semenov and Y. M. Beltukov, *Int. J. Solids Struct.* **191-192**, 333 (2020).
- [39] M. S. Alnæs, J. Blechta, J. Hake, A. Johansson, B. Kehlet, A. Logg, C. Richardson, J. Ring, M. E. Rognes, and G. N. Wells, *Arch. Numer. Softw.* **3**, 9 (2015).
- [40] T. Mori and K. Tanaka, *Acta Metall.* **21**, 571 (1973).
- [41] Y. Benveniste, *Mech. Mater.* **6**, 147 (1987).
- [42] J. Cho, M. S. Joshi, and C. T. Sun, *Compos. Sci. Technol.* **66**, 1941 (2006).
- [43] V. K. Malinovsky and A. P. Sokolov, *Solid State Commun.* **57**, 757 (1986).
- [44] H. Shintani and H. Tanaka, *Nat. Mater.* **7**, 870 (2008).
- [45] C. S. O'Hern, L. E. Silbert, A. J. Liu, and S. R. Nagel, *Phys. Rev. E* **68**, 011306 (2003).
- [46] M. Wyart, *Europhys. Lett.* **89**, 64001 (2010).
- [47] E. DeGiuli, A. Laversanne-Finot, G. Düring, E. Lerner, and M. Wyart, *Soft Matter* **10**, 5628 (2014).
- [48] E. De Giuli, E. Lerner, and M. Wyart, *J. Chem. Phys.* **142**, 164503 (2015).
- [49] E. Lerner, E. DeGiuli, G. Düring, and M. Wyart, *Soft Matter* **10**, 5085 (2014).